AN APPLICATION OF FINITE ELEMENT METHOD TO SOIL-FOUNDATION INTERACTION ANALYSES

Eiichi Kuribayashi* and Yutaka Iida**

ABSTRACT

This paper discusses the soil-foundation interaction of an actual structure. The Kanmon Bridge, completed in November 1973, is a three span suspension bridge with 712m center span crossing over the Kanmon Strait between Shimonoseki in Honshu main island and Moji in Kyushu island. During the construction period dynamic field tests on both of the foundations of two main towers were carried out. The Shimonoseki-side foundation, 40m wide, 20m long and 14m deep, weighs about 25,000t and the Moji-side foundation, 40m wide, 20m long and 30m deep, weighs about 50,000t. Their bottoms reach to sound rock layers. Sinusoidal vibratory horizontal forces, up to 35t at 5.5c/s and 40t at 12c/s, were applied to the tops of the foundations. Several peaks appear in resonance curves. In considering the appearance of these peaks, interaction between the structure and the surrounding ground should be taken into consideration. Some analyses were conducted to estimate elastic moduli of the soils and to obtain dynamic characteristics of the Moji-side foundation. From the tests and the analyses the following may be concluded.

1) Elastic moduli of the soils are considerably greater (about 5 times) than those used in the design, therefore displacement due to seismic excitations during future earthquakes may be smaller than those expected in the design.

2) In discussing dynamic characteristics of huge foundations it is necessitated to consider the effects of geological and topographical features and of adjacent structures. And dynamic characteristics of those structures can be satisfactorily obtained by a response analysis on the basis of the finite element method.

1. INTRODUCTION

The Kanmon Bridge, completed in November 1973, is a three span suspension bridge with 712 m center span crossing over the Kanmon Strait between Shimonoseki in Honshu main island and Moji in Kyushu island. The location and the general view are shown in Figs. 1 and 2, respectively.

The modified seismic coefficient method considering structural response applies to its earthquake resistant design. The basic seismic coefficients are taken as 0.15 horizontally and 0.075 vertically.

To obtain the dynamic properties of the bridge, field vibration tests on both of the foundations of the two main towers, the so-called main piers, were carried out in July 1970 and on the Moji main tower in May 1971. Statical and dynamical testing of the whole bridge was conducted in September, 1973 and now long term seismic observations have been made on it.

In this paper the results of field vibration tests on the piers and some soil-foundation interaction analyses are presented.

* Chief, Earthquake Engineering Research Section, Public Works Research Institute, Ministry of Construction, Japan.
** Research Engineer, do.

2. RESULTS OF FIELD VIBRATION TESTS

The cross sections of the two piers, i.e. the Shimonoseki pier and the Moji pier, are shown in Figs. 3 and 4. The Shimonoseki pier, 40 m wide, 20 m long and 14 m deep, weighs about 25,000t and the Moji pier, 40 m wide, 20 m long and 30 m deep weighs about 50,000t. Their bottoms reach to sound rock layers.

Sinusoidal vibratory horizontal forces, up to 35t at 5.5 c/s and 40t at 12 c/s were applied to the tops of the pier in the longitudinal or transverse direction.

The typical relations between the amplitude or phase angle and the frequency enforced are shown in Fig. 5 to Fig. 12. A resonant frequency for the Shimonoseki site shifts away the frequency range of this testing and several resonance peaks appear for the Moji site.

In considering the appearance of the several peaks, interaction between the structure and the surrounding soil should be taken into consideration and in macroscopic view, two peaks are observed in Fig. 10.

3. ESTIMATIONS OF ELASTIC MODULI OF SOILS

To estimate elastic moduli of the soils in the tests, a two degree of freedom model shown in Fig. 13 was employed. The model

consists of a rigid body and supporting springs which represent the pier and the subsoils, respectively.

When a sinusoidal vibratory horizontal force F cos ωt is applied to the top of the pier, the equations of motion are as follows.

$$M\ddot{x} + K_H (x - l_H \theta) + K_S (x - l_S \theta) = F \cos \omega t \quad (1)$$

$$J\ddot{\theta} + K_\theta \theta - K_H l_H (x - l_H \theta) - K_S l_S (x - l_S \theta) = F l_f \cos \omega t \quad (2)$$

where

M	: Mass of the pier
J	: Rotational inertia of the pier around the axis of gravity
K_H	: Spring constant due to the subsoil reaction at the side of the pier in the horizontal direction.
K_S	: Spring constant due to the subsoil reaction at the bottom of the pier in the horizontal direction
l_H	: Distance between the level of the center of gravity and the side spring
l_S	: Distance between the center of gravity and the bottom of the pier
l_f	: Distance between the center of gravity and the top of the pier
l_O	: Distance between the center of gravity and the center of rotation
F	: Amplitude of the exciting force
ω	: Exciting circular frequency
x	: Horizontal displacement of the center of gravity
θ	: Rotational displacement of the pier

The relations between spring constants and elastic moduli of soils can be determined by using F. Vogt's solution.

It is known that resonance curves become almost flat and approach to the static displacements in the sufficiently low frequency range below fundamental natural frequencies.

Assuming ω = 0 in Eqs. (1) and (2), one obtains the equations of static equilibrium.

Using the amplitudes of resonance curves from the tests in the low frequency range and the equations of static equilibrium, one can estimate the elastic moduli of the soils.

The elastic moduli estimated and the ones for design are shown in Figs. 14 and 15. The elastic moduli from the vibration tests are close to the ones from the shear wave velocities shown in Table 1.

4. SOIL-FOUNDATION INTERACTION ANALYSES ON THE BASIS OF THE FINITE ELEMENT METHOD

It is assumed that the damping matrix (C) can be transformed to a diagonal matrix by the modal matrix (Φ) in the equation of motion of an n degree of freedom system. In the case that the j th component R_j of the applied load column vector is set equal to F cos ωt and the others to zeros, the forced vibration part r_k of the k th component of the displacement column vector is expressed in the following form.

$$r_k = \sum_{i=1}^{n} \phi_k^{(i)} \xi_i(t)$$

$$= \frac{F}{\bar{m}} \sum_{i=1}^{n} \phi_k^{(i)} \phi_j^{(i)} \frac{1}{(p_i^2 - \omega^2)^2 + 4n_i^2 \omega^2} \times \{(p_i^2 - \omega^2) \cos \omega t + 2n_i \omega \sin \omega t\}$$

$$= \frac{F}{\bar{m}} \cos \omega t \sum_{i-1}^{n} \phi_k^{(i)} \phi_j^{(i)} \times \frac{(p_i^2 - \omega^2)}{(p_i^2 - \omega^2)^2 + 4n_i^2 \omega^2} + \frac{F}{\bar{m}} \sin \omega t \sum_{i=1}^{n} \phi_k^{(i)} \phi_j^{(i)} \times \frac{2n_i \omega}{(p_i^2 - \omega^2)^2 + 4n_i^2 \omega^2}$$

$$= \frac{F}{\bar{m}} \sqrt{\left\{\sum_{i=1}^{n} \phi_k^{(i)} \phi_j^{(i)} \frac{p_i^2 - \omega^2}{(p_i^2 - \omega^2)^2 + 4n_i^2 \omega^2}\right\}^2 + \left\{\sum_{i=1}^{n} \phi_k^{(i)} \phi_j^{(i)} \frac{2n_i \omega}{(p_i^2 - \omega^2)^2 + 4n_i^2 \omega^2}\right\}^2} \times \cos(\omega t - \phi) \quad (3)$$

where

$$\phi = \tan^{-1} \left\{ \frac{\sum_{i=1}^{n} \phi_k^{(i)} \phi_j^{(i)} \frac{2n_i \omega}{(p_i^2 - \omega^2)^2 + 4n_i^2 \omega^2}}{\sum_{i=1}^{n} \phi_k^{(i)} \phi_j^{(i)} \frac{p_i^2 - \omega^2}{(p_i^2 - \omega^2)^2 + 4n_i^2 \omega^2}} \right\} \quad (4)$$

$\phi_k^{(i)}$	: k th component of the shape column vector $\{\phi^{(i)}\}$ for the i th mode
$\xi_i(t)$	: i th normal coordinate
p_i	: i th natural circular frequency
n_i	: i th damping constant
$\bar{m}$	: $\{\phi^{(i)}\}^T$ (M) $\{\phi^{(i)}\}$
(M)	: Mass matrix

In the static case the j th component Rj of the applied load column vector is set equal to F and the others to zero, the k th component r_k^S of the static displacement column vector is expressed in the form:

$$r_k^s = \frac{F}{\bar{m}} \sum_{i=1}^{n} \phi_k^{(i)} \phi_j^{(i)} \frac{1}{p_i^2} \qquad (5)$$

Using eqs. (3), (4) and (5), one can obtain resonance and phase angle curves analytically.

In the case of the Moji pier in the longitudinal direction the analyses were carried out. The finite element idealization is shown in Fig. 16. The load is applied at the node 3. Modes and static displacements are shown in Figs. 17 to 25. The resonance and phase angle curves shown in Figs. 26, 27 and 28 correspond to the curves shown in Figs. 10, 11 and 12, respectively. The damping ratio h=n/p is set equal to 10% for each mode.

It may be remarked that the analytical results correspond to the test results fairly well.

5. CONCLUSION

From the tests and the analyses the following may be concluded.

1) Elastic moduli of the soils are considerably greater (about 5 times) than those used in the design, therefore displacement due to seismic excitations during future earthquakes may be smaller than those expected in the design.

2) In discussing dynamic characteristics of huge foundations it is necessitated to consider the effects of geological and topographical features and of adjacent structures. And dynamic charactertistics of those structures can be satisfactorily obtained by a response analysis on the basis of the finite element method.

6. ACKNOWLEDGEMENT

The authors wish to express their appreciation to the staffs of Earthquake Engineering Research Section, Public Works Research Institute and the members of Japan Highway Public Corporation for their efforts in the vibration tests.

7. REFERENCES

Japan Highway Public Corporation, "The Kanmon Bridge," January 1974.

United States Department of the Interior, Bureau of Reclamation, "Treatise on Dams, Design Supplement No. 2, Charter 10 Arch Dams (2) Foundation Constant", 1934.

Vogt, Fredrik, "Uber die Berechnung der Fundament-deformation," Det Norske Bidenskaps Akademi, Oslo, 1925.

TABLE 1.

YOUNG'S MODULI OF SOILS FROM SHEAR WAVE VELOCITIES

		Shimonoseki Side	Moji Side
1st Layer	Depth (m)	5 ∿ 10	5 ∿ 10
	Shear Wave Velocities (Km/sec)	0.3 ∿ 0.4	0.3
	Young's Moduli (t/m^2)	$0.5 \sim 1.0 \times 10^5$	
2nd Layer	Depth (m)	10 ∿ 25	10 ∿ 30
	Shear Wave Velocities (Km/sec)	0.7 ∿ 1.5	1.0 ∿ 1.3
	Young's Moduli (t/m^2)	$0.5 \sim 1.5 \times 10^6$	
3rd Layer	Depth (m)	-	-
	Shear Wave Velocities (Km/sec)	4.0 ∿ 4.7	4.5 ∿ 4.7
	Young's Moduli (t/m^2)	$0.9 \sim 1.3 \times 10^6$	

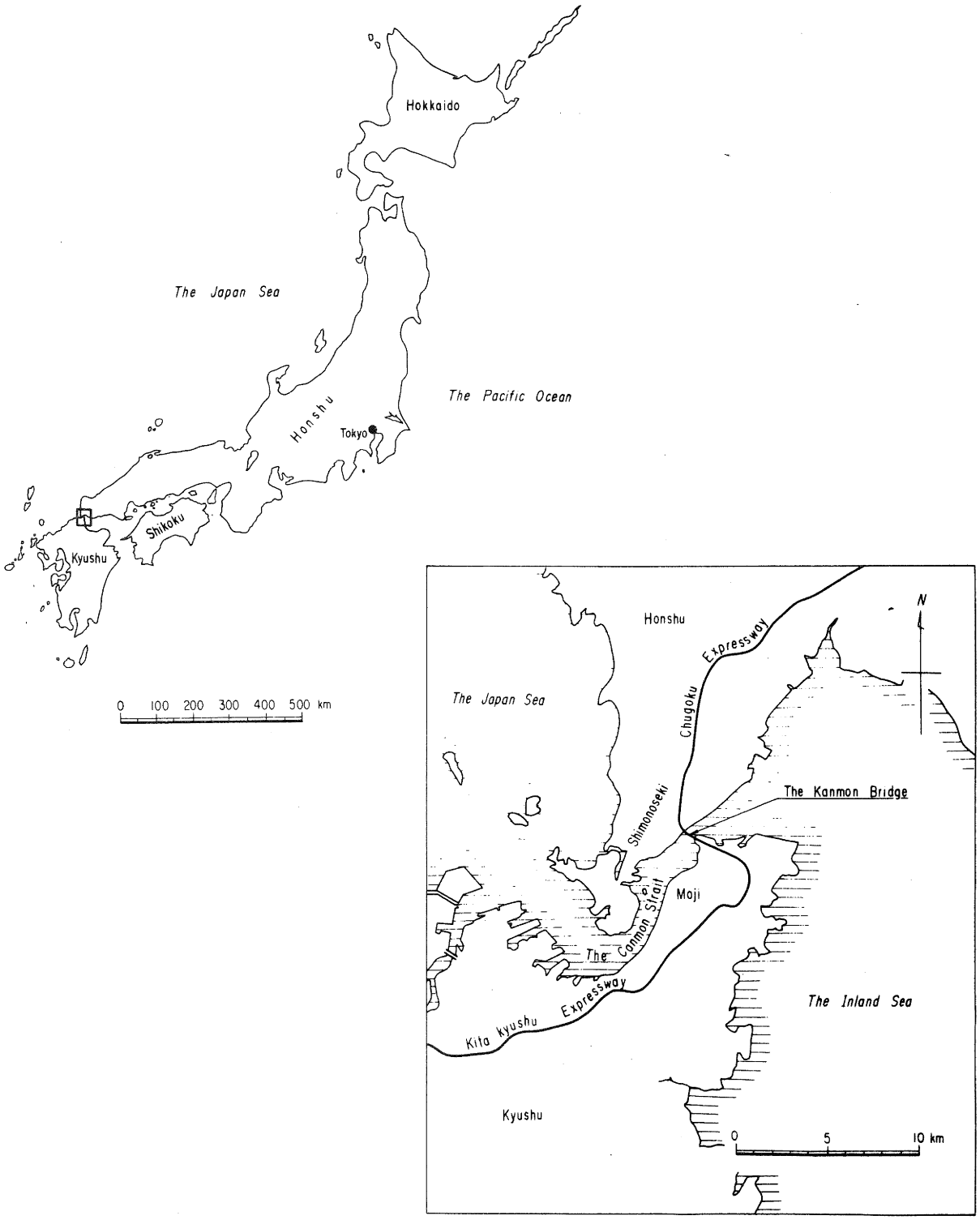

Fig. 1 LOCATION OF THE KANMON BRIDGE

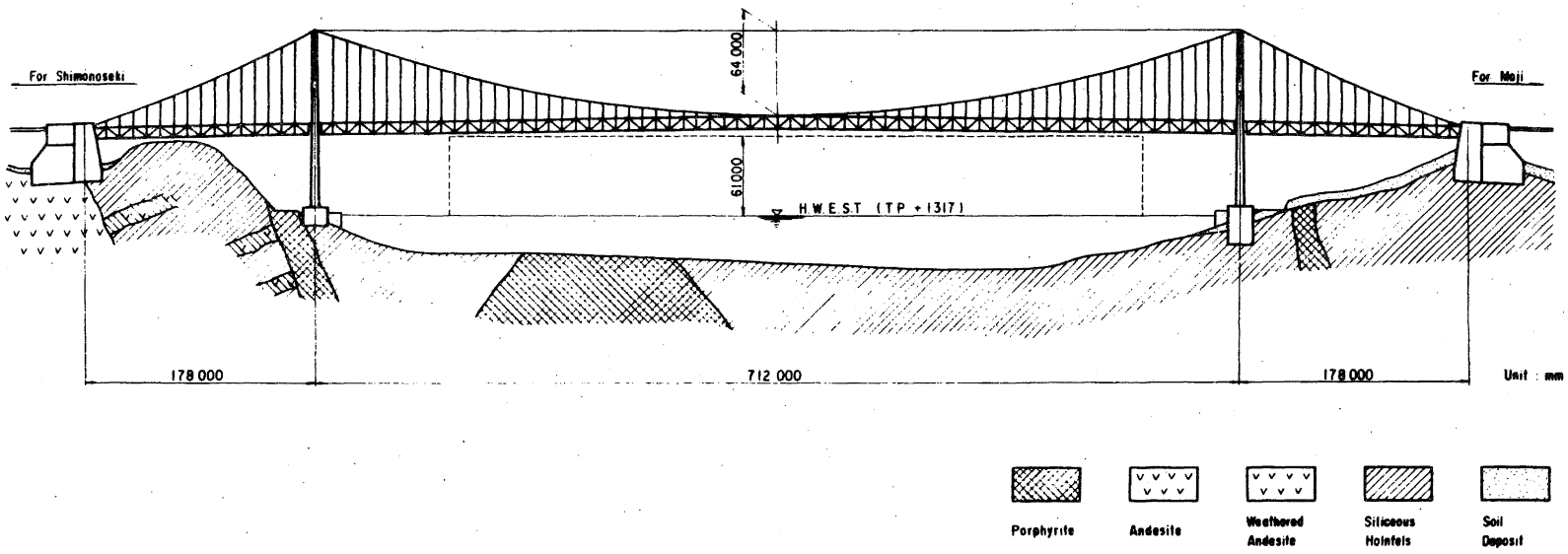

Fig. 2 GENERAL VIEW OF THE KANMON BRIDGE

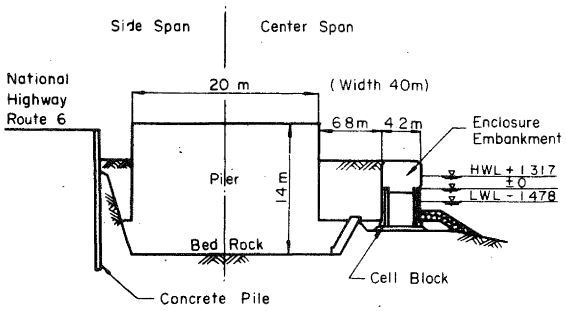

Fig. 3 CROSS SECTION OF THE SHIMONOSEKI PIER

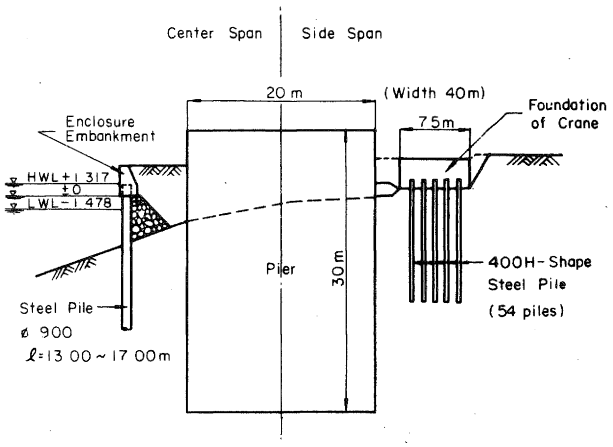

Fig. 4 CROSS SECTION OF THE MOJI PIER

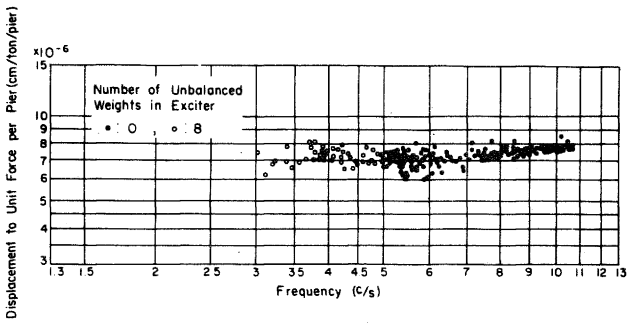

Fig. 5 RESONANCE CURVE AT THE TOP OF THE SHIMONOSEKI PIER-LONGITUDINAL

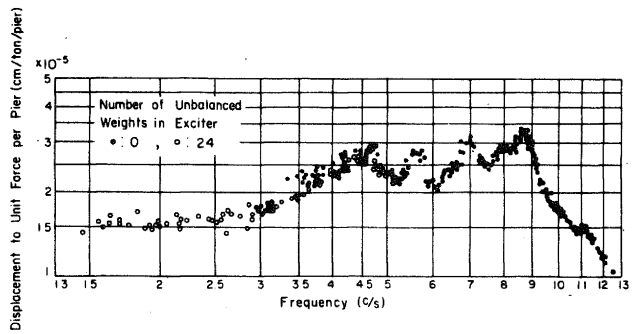

Fig. 6 RESONANCE CURVE AT THE TOP OF THE MOJI PIER-TRANSVERSE

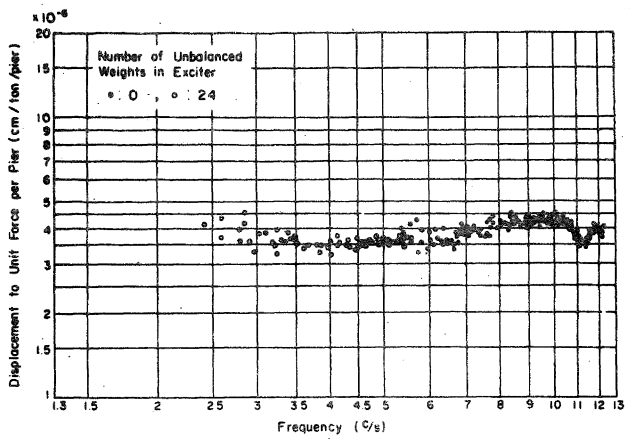

Fig. 7 RESONANCE CURVE AT THE TOP OF THE SHIMONOSEKI PIER-TRANSVERSE

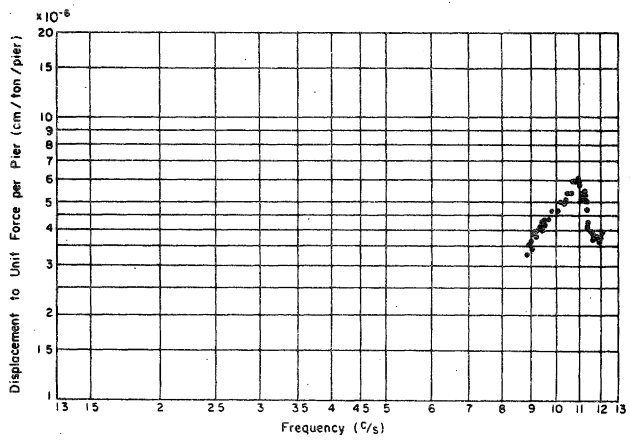

Fig. 8 RESONANCE CURVE ON THE SHIMONOSEKI ENCLOSURE EMBANKMENT-TRANSVERSE

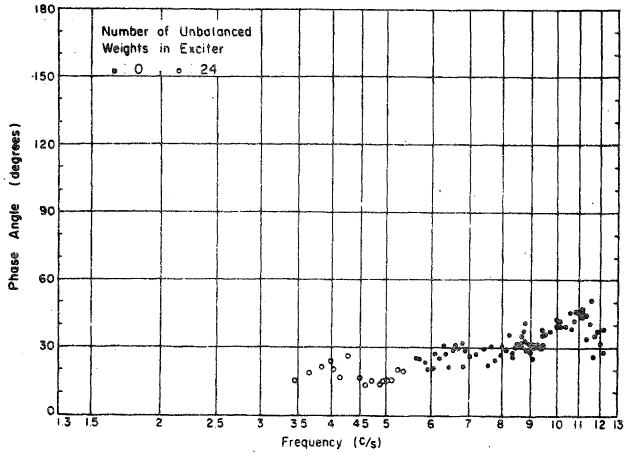

Fig. 9 PHASE ANGLE CURVE AT THE TOP OF THE SHIMONOSEKI PIER-TRANSVERSE

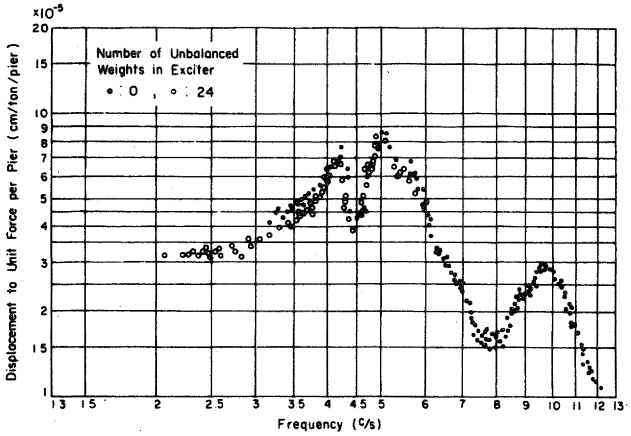

Fig. 10 RESONANCE CURVE AT THE TOP OF THE MOJI PIER-LONGITUDINAL

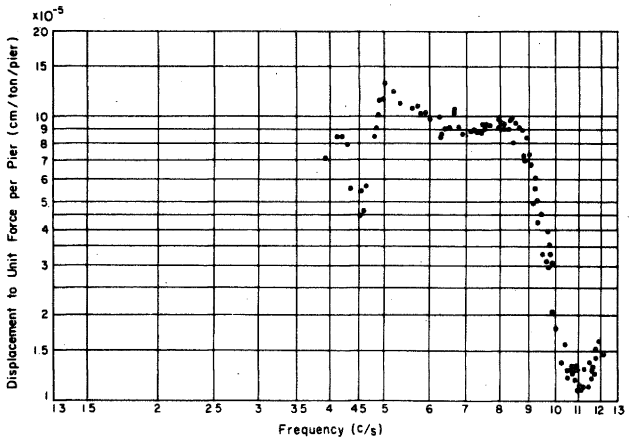

Fig. 11 RESONANCE CURVE ON THE MOJI ENCLOSURE EMBANKMENT-LONGITUDINAL

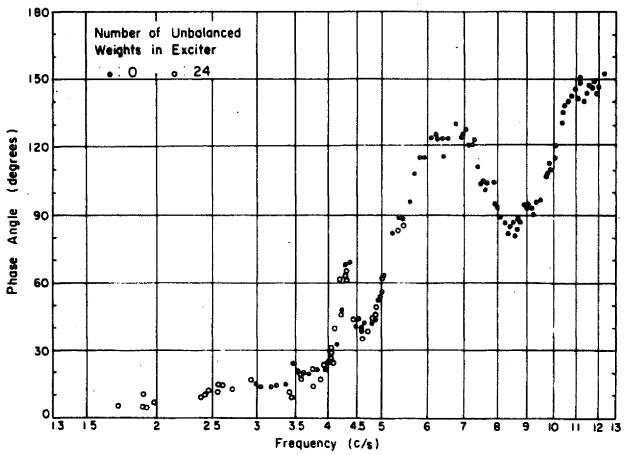

Fig. 12 PHASE ANGLE CURVE AT THE TOP OF THE MOJI PIER-LONGITUDINAL

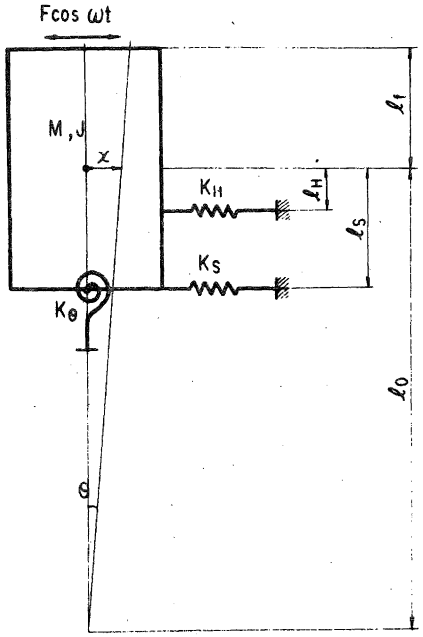

Fig. 13 TWO DEGREE OF FREEDOM MODEL

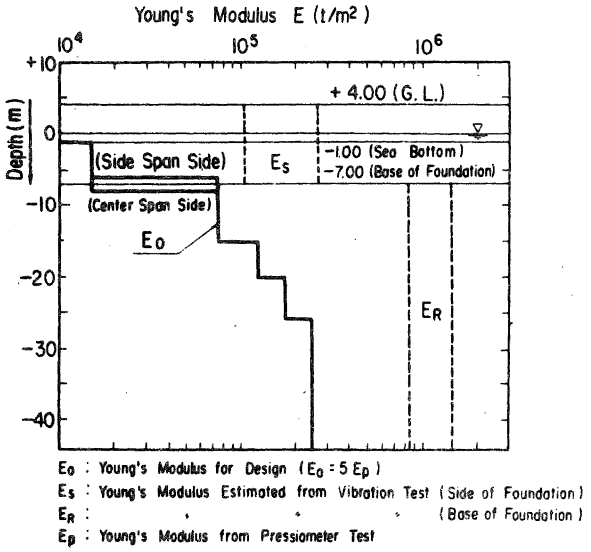

Fig. 14 YOUNG'S MODULI OF SOILS AT THE SHIMONOSEKI SITE

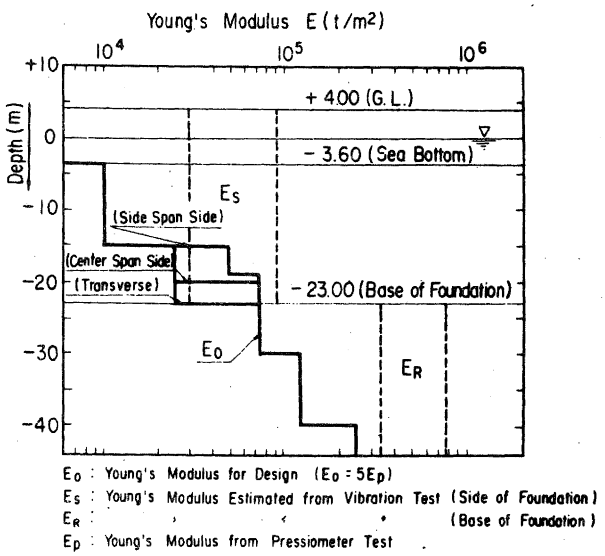

Fig. 15 YOUNG'S MODULI OF SOILS AT THE MOJI SITE

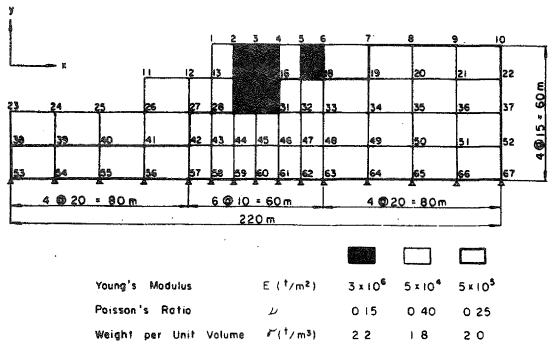

Fig. 16 FINITE ELEMENT IDEALIZATION

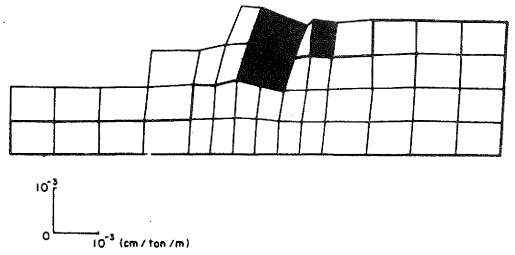

Fig. 17 STATIC DISPLACEMENT DUE TO THE HORIZONTAL FORCE AT THE NODE NO. 3

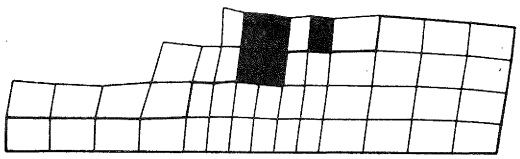

Fig. 18 1st MODE f = 3.69 C/S

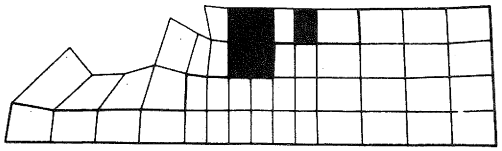

Fig. 19 2nd MODE f = 4.33 C/S

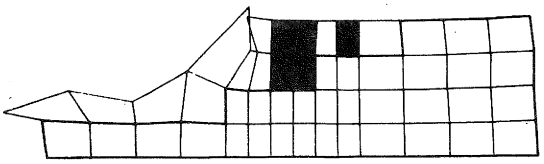

Fig. 20 3rd MODE f = 4.62 C/S

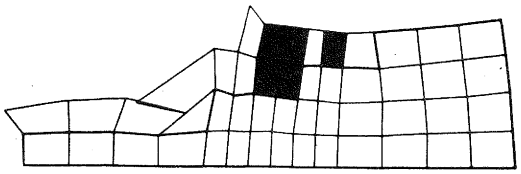

Fig. 21 4th MODE f = 5.40 C/S

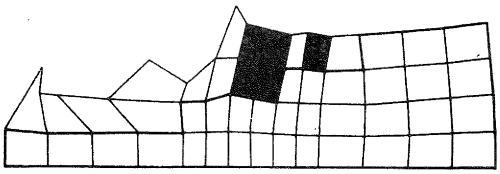

Fig. 22 5th MODE f = 5.88 C/S

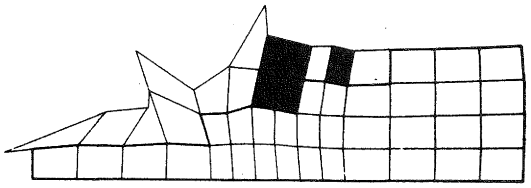

Fig. 23 6th MODE f = 6.53 C/S

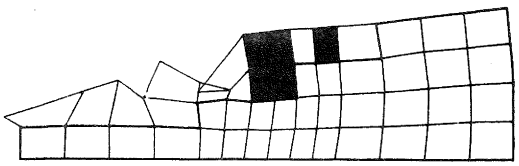

Fig. 24 7th MODE f = 6.70 C/S

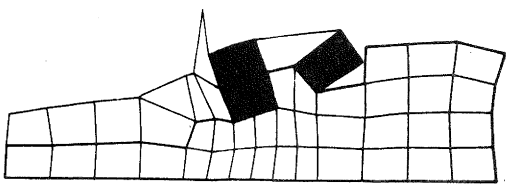

Fig. 25 21st MODE f = 10.17 C/S

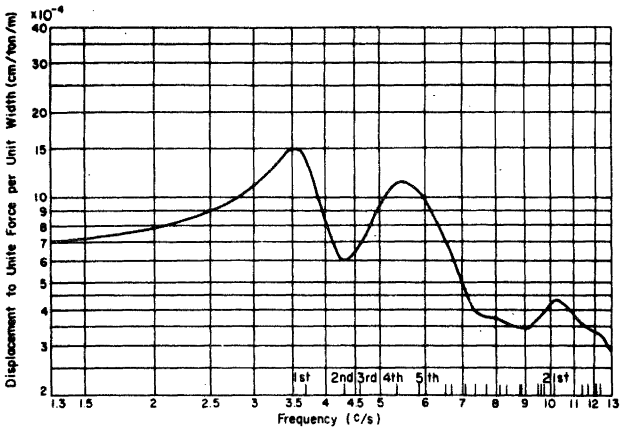

Fig. 26 RESONANCE CURVE AT THE NODE NO. 3

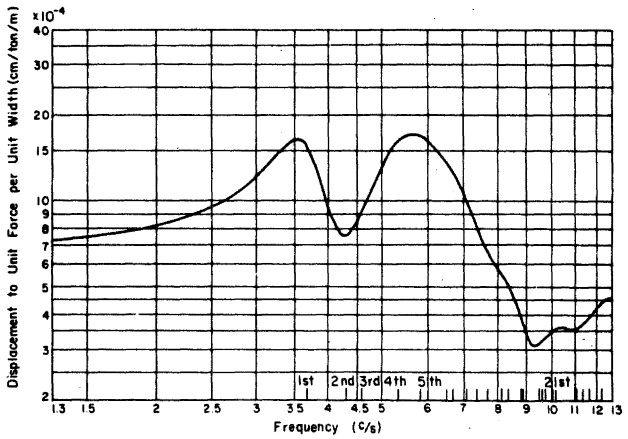

Fig. 27 RESONANCE CURVE AT THE NODE NO. 1

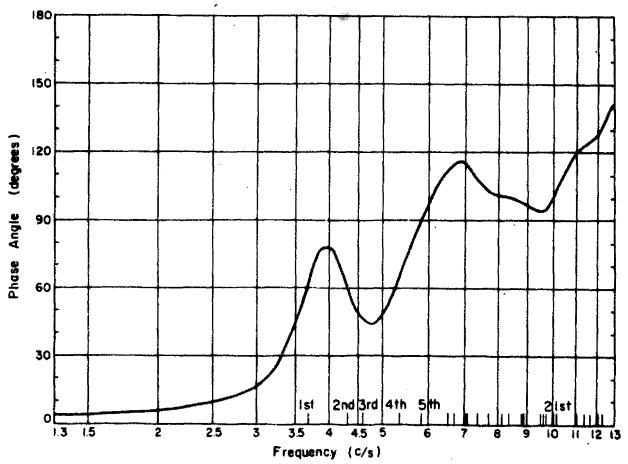

Fig. 28 PHASE ANGLE CURVE AT THE NODE NO. 3